Available online at www.sciencedirect.com

ScienceDirect

Energy Procedia 91 (2016) 668 – 680

Energy Procedia

SHC 2015, International Conference on Solar Heating and Cooling for Buildings and Industry

Targeting optimal design and operation of solar heated industrial processes: a MILP formulation

Anna S. Wallerand[a]*, Angelos Selviaridis[b], Araz Ashouri[a], François Maréchal[a]

[a]*École Polytechnique Fédéral de Lausanne, STI-IGM-IPESE, Case Postale 440, 1951 Sion, Switzerland*
[b]*Airlight Energy Holding SA, Via Industria 10, 6710 Biasca, Switzerland*

Abstract

The intermittence of solar irradiation displays a great challenge for industrial applications, which often require a constant heat supply. Transient or dynamic simulation software, such as TRNSYS and EnergyPlus, enable modeling of such systems and the respective dynamic responses. Design and operation in these software packages is usually based on heuristic strategies.
In this work, optimal design and operation of a solar heated industrial process with constant heating requirements is investigated based on Mixed Integer Linear Programming (MILP). The MILP model is constrained by surrogate functions that capture the main inefficiencies, but do not represent the dynamic behavior. In order to investigate the dynamic behavior and feasibility of the results from MILP, a TRNSYS model is created. In this way, the MILP model is verified and the quality of the dynamic model can be evaluated with respect to the potential non-dynamic optimum.
The industrial heating requirements between 60 and 80°C are satisfied with the help of a novel High Concentration Photovoltaic Thermal System (HCPVT), a stratified thermal storage tank, and a back-up burner. The system is evaluated for Sede Boqer, Israel, and Tateno, Japan, two differently featured locations. It is concluded that the MILP formulation supplies a satisfying approximation of the system performance and, hence, may supply satisfying estimates of the system design and operation. It may also be concluded, that heuristic design and operation strategies can generate very good solutions with respect to the theoretical optimum. In this work, the system is optimized with respect to the thermal behavior and efficiency, and not the economic aspects.

Peer-review by the scientific conference committee of SHC 2015 under responsibility of PSE AG

Keywords: Mixed Integer Linear Programming MILP; solar heating; industrial process; dynamic simulation; TRNSYS; stratified thermal storage tank;

* Corresponding author. Tel.: +41 21 69 58261
*E-mail address:*anna.wallerand@epfl.ch

Peer-review by the scientific conference committee of SHC 2015 under responsibility of PSE AG
doi:10.1016/j.egypro.2016.06.229

1. Introduction

Solar heating and cooling applications and their system design optimization is a widely discussed topic not only due to the related environmental benefits. According to Henning et al. (1) the main obstacle against large-scale application is the lack of practical knowledge on design, control and operation of such systems. Dynamic modeling of solar heating and cooling applications is commonly addressed with transient system simulation software such as TRNSYS (2-7), INSEL (8), EnergyPlus (9) or Polysun (10). These allow dynamic analysis and performance evaluation of a specific design configuration. A heuristic way to improve the design is by varying the value of each variable while keeping the others unchanged in order to see the effect on the objective function. The approach is referred to as 'parametric simulation method' (11) and is applied for system enhancement (6).

A number of internal or external 'plug-in' toolboxes (DAKOTA (12), GenOpt (13)) enable optimization of the operating conditions and component sizes of dynamic models. Dynamic models are usually non-linear and generate discontinuous output due to the nature of the simulation software solvers or empirically assigned inputs. Stochastic methods are therefore the most commonly applied optimization algorithms (Genetic Algorithms (5, 14, 15), Particle Swarm Optimization (16)). As these heuristic algorithms often require hundreds or thousands of evaluations, computationally expensive models cannot be treated. Surrogate models, e.g. based on Artificial Neural Networks (ANN) (5, 17), provide a solution.

The above presented methodologies allow dynamic system design, analysis, and optimization based on heuristic, often computationally expensive methods that do not always guarantee finding an optimum.

On the other hand, Mixed Integer Linear Programming (MILP) methods have been used by many researchers for optimal design and control of integrated energy systems with industrial application (18-20), for building services (21, 22), urban planning (23, 24), and thermal storages (25-27). Solar technologies are considered in some of these (19, 21). The suitability of MILP for optimization problems is demonstrated by Bemporad et al. (28). One challenge of MILP problem formulations is the reduction of the problem to linear equations. Several solutions for dealing with this impediment, such as Taylor series expansion, are investigated for a thermal storage unit in (26) at the cost of higher computational effort.

System behavior representation in sufficient accuracy of the MILP model at reasonable computational effort is tackled in this work for a solar thermal system coupled with a stratified thermal storage tank for heat supply to a continuous industrial process represented by a constant demand. Three different MILP formulations are presented and compared. A TRNSYS model of the same problem is created and used for tuning of parameters in the MILP formulation as well as for testing the optimal set of variables. Special attention is put on the storage equations, since the thermal storage behavior may be crucial to solar applications especially for constant demands imposed by an industrial demand.

Nomenclature

A	surface area [m^2]
c_p	heat capacity [kJ/kgK]
$\dot{Q}$	thermal power [kW]
Q	thermal energy [kWh]
T	temperature [°C]
U	heat transfer coefficient [W/m^2]
α	linear coefficient: slope
β	linear coefficient: intercept
η	efficiency [-]
κ	parameter [-]
ρ	density [kg/m^3]

Abbreviations

AUX	Auxiliary heater

BSRN	Baseline Surface Radiation Network
DISH	HCPVT dish
DNI	Direct Normal Radiation [W/m^2]
HCPVT	High Concentration Photovoltaic and Thermal System
DEM	Industrial demand
MILP	Mixed Integer Linear Programming
SBO	Sede Boqer (BSRN weather station)
STOR	Thermal storage
TAT	Tateno (BSRN weather station)

2. System and methods description

The system consists of a novel High Concentration Photovoltaic Thermal (HCPVT) (29-31) dish that provides solar heat to an industrial process (between 60 and 80°C) and to a stratified thermal storage tank. The stratified tank is connected to the system via two bypass loops. The industrial demand is connected to the solar circuit through a heat exchanger. The HCPVT produces electricity and hot water at 85°C with an electrical and thermal efficiency of 31.1% and 55% respectively. Characteristics of the HCPVT are the high concentration (2000 suns) and the low thermal inertia and the accompanying fast temperature response, which means that the desired outlet temperature can be reached within short time frame, even for weak DNI values (29). At the same time it is necessary to keep the PV cell temperature within safety limits to avoid damage. The electrical output is not treated in this work. Due to two-axis tracking, the collector output is not subject to cosine losses in winter.

2.1. Radiation data

Historic radiation data of a full year is retrieved from the Baseline Surface Radiation Network (BSRN) (32) in minute wise time resolution (for the TRNSYS model) and hourly resolution (for the MILP model). This is justified by the desire for most realistic observations. For future analysis a typical meteorological year (TMY) is also recommended. The analysis is carried out for two weather stations with different meteorological topology. Sede Boqer (Israel) lies in the Har Hanegev desert, which is a comparatively dry region with high yearly Direct Normal Radation (DNI) (2208 kWh, 2011 (32)). It provides a good example for an isolated area that could profit from solar energy supply. On the other hand, Tateno (Japan) has a humid subtropical climate, a distinctly lower DNI (1164 kWh, 2011 (32)), and a more moderate seasonal variation. Investigation of both locations allows a more holistic view on the system performance and methods.

2.2. Dynamic model

The system components and connections of the TRNSYS 17 (33) model are depicted in Fig. 1. For simplicity, controllers and equations are not displayed. The units indicated with a small arrow are the units exposed to control signals. The component sizes and parameters of the initial case are displayed in Table 1.

The variable speed pump, which circulates the solar-to-demand circuit, is controlled by an iterative feedback controller. It ensures that the inlet temperature to the solar receiver is kept constant such that the photovoltaic cell cannot be harmed. This leads to small variations of the inlet temperature of the storage/demand. The controlled flow diverter in the storage bypass is operated in such a way that satisfying the demand with direct solar energy is always prioritized towards filling of the storage. The storage discharge pump controls the mass flow rate such that the storage bottom inlet temperature remains constant. This temperature constrained control reacts to the decrease in storage outlet temperature by reducing the mass flow rate accordingly.

The initial component sizes are determined by general reasoning. The HCPVT has a rated thermal power output of 22kW$_{th}$ and 12 kW$_{el}$ at a DNI of 1000W/m^2. The original industrial demand size is chosen to be half of the rated solar thermal output. The storage is sized for the day of highest solar radiation with the assumption everything that is not consumed during that time is stored (day of highest DNI: 196, 13.6 h of sunshine, 3.2 m^3).

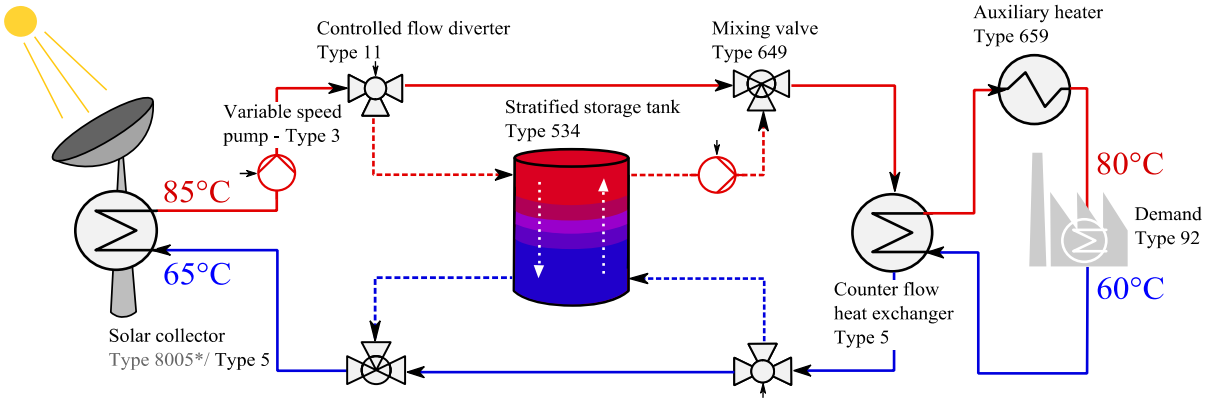

Fig. 1 System layout with TRNSYS components.

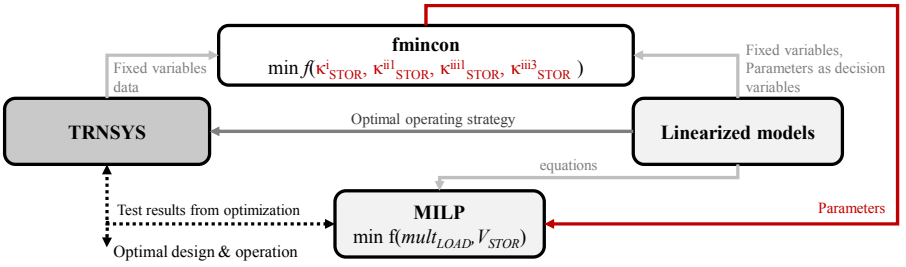

Fig. 2 Methodology for finding the surrogate parameters, and the system optimal design and operation.

Table 1 TRNSYS data sheet for the reference case of Sede Boqer.

	Symbol	Value	Unit		Symbol	Value	Unit
Fluid specific heat	c_p	4.2	kJ/kgK	Heat exchanger	Type 5		
Fluid density	ρ	990	kg/m^3	Heat transfer coefficient		3150	W/K
Fluid thermal conductivity		0.5944	W/mK	Counter flow mode		2	-
Fluid thermal Expansion coeff.		0.00026	1/K	Auxiliary heater / Demand	Type 659/92		
Storage	Type 534			Rated capacity		20	kW
Tank volume		3.0	m^3	Demand	$\dot{Q}_{DEM}$	10.1	kW
Height		1.9	m	HCPVT dish (user created)	Type 8050		
Top/bottom/side loss coefficient	U	1.5	W/m^{2}K	Electrical efficiency	η_{el}	0.311	-
Number of nodes		10	-	Thermal efficiency	η_{th}	0.55	-
Initial node temperature		20	C	Collector area	A_{coll}	40	m^2

Table 2 Parameters of different MILP cases as fit with the data for Sede Boqer.

Parameter	Value	Parameter	Value	Parameter	Value	Parameter	Value	Parameter	Value
κ^{i}_{STOR}	0.92	κ^{iii1}_{STOR}	0.95	$mult^{min}_{DEM}$	0	Q^{MAX}_{STOR}	1e3kWh	T^{h}_{STOR}	85°C
κ^{ii1}_{STOR}	0.96	κ^{iii3}_{STOR}	0.93	$mult^{max}_{DEM}$	2	T_{STOR}	80°C	T^{c}_{STOR}	65°C
Q_{DEM}	10.1 kW	Q^{max}_{DISH}	22 kW	A_{DISH}	40 m^2	η_{el}	0.311	η_{th}	0.55

2.3. Mixed Integer Linear Programming (MILP) formulation

The set of linear equations used to describe thermal behavior of the solar dish, the thermal storage, the auxiliary heater, and industrial demand is presented in this section. Scalar decision variables are henceforth represented by italic letters and parameters by roman letters; vectors are depicted in bold (with italic for variables or roman for parameters). In order to keep the problem size reasonable, the MILP equations are set in hourly resolution. The data set is chosen for the whole year instead of a set of typical periods (34), in order to keep origin of the errors traceable.

2.3.1. High Concentration Photovoltaic and Thermal (HCPVT) dish

The HCPVT dish is modelled by a simple set of equations based on the thermal and electrical efficiency. The solar dish is connected directly to the demand by a bypass loop and to the thermal storage unit. The transfer rates between solar and demand or storage are decision variables.

$$\begin{aligned}&\dot{\mathbf{Q}}_{\mathbf{DISH}} = \eta^{\mathrm{th}}_{\mathrm{DISH}} \cdot \mathrm{A}_{\mathrm{DISH}} \cdot \mathbf{DNI} \\ &\dot{\mathbf{Q}}_{\mathbf{DISH}} = \dot{\boldsymbol{Q}}_{\boldsymbol{DISH\rightarrow STOR}} + \dot{\boldsymbol{Q}}_{\boldsymbol{DISH\rightarrow DEM}}\end{aligned} \tag{1}$$

2.3.2. Industrial demand and auxiliary heater

The industrial demand is, as mentioned before, set to a constant value. Heat is delivered from the solar dish, the storage, and an auxiliary heater, which ensures fulfillment of the requirements. A decision variable is introduced to the equation which may be used to size the demand optimally ($mult_{DEM}$). Initially it is set to one.

$$\dot{\mathrm{Q}}_{\mathrm{DEM}} \cdot mult_{DEM} = \dot{\boldsymbol{Q}}_{\boldsymbol{DISH\rightarrow DEM}} + \dot{\boldsymbol{Q}}_{\boldsymbol{STOR\rightarrow DEM}} + \dot{\boldsymbol{Q}}_{\boldsymbol{AUX}} \tag{2}$$

2.3.3. Thermal storage

For the stratified storage tank three different approaches are evaluated. The first one is based on an ideal stratified tank formulated in (27) with an additional parameter for the global losses which account for thermal losses as well as de-stratification. The other storage models contain further refinement.

2.3.3.1 Storage model (i)

The energy balance (i) of the ideal stratified storage tank assumes that the storage content of time t depends on the previous storage level (t-1) multiplied by a thermal loss fraction, the inflow and outflow at time t.

$$\begin{aligned}&\mathbf{T} = \{1,2,...,8760\} \\ &\boldsymbol{Q}^{\boldsymbol{i}}_{\boldsymbol{STOR}}(t) = \boldsymbol{Q}^{\boldsymbol{i}}_{\boldsymbol{STOR}}(t-1) \cdot \kappa^{\mathrm{i}}_{\mathrm{STOR}} + \left(\dot{\boldsymbol{Q}}_{\boldsymbol{DISH\rightarrow STOR}}(t) - \dot{\boldsymbol{Q}}_{\boldsymbol{STOR\rightarrow DEM}}(t)\right) \cdot \mathrm{dt} \quad \forall t \in \mathbf{T} \setminus \{1\} \\ &\boldsymbol{Q}^{\boldsymbol{i}}_{\boldsymbol{STOR}}(1) = 0 = \left(\dot{\boldsymbol{Q}}_{\boldsymbol{DISH\rightarrow STOR}}(1) - \dot{\boldsymbol{Q}}_{\boldsymbol{STOR\rightarrow DEM}}(1)\right)\end{aligned} \tag{3}$$

$$\begin{aligned}&0 \le Q^{i,\max}_{STOR} \le \mathrm{Q}^{\mathrm{MAX}}_{\mathrm{STOR}} \\ &0 \le \kappa^{\mathrm{i}}_{\mathrm{STOR}} \le 1\end{aligned} \tag{4}$$

2.3.3.2 Storage model (ii)

Model (i) accounts for thermal losses proportional to the storage energy content. However thermal losses are normally formulated as a function of the tank surface area, the heat transfer coefficient, and the inside and outside temperatures. Therefore, a term accounting for constant thermal losses independent from the filing level is added to the equation.

$$\boldsymbol{Q}^{\boldsymbol{ii}}_{\boldsymbol{STOR}}(t) = \boldsymbol{Q}^{\boldsymbol{ii}}_{\boldsymbol{STOR}}(t-1) \cdot \kappa^{\mathrm{ii}_1}_{\mathrm{STOR}} + \left(\dot{\boldsymbol{Q}}_{\boldsymbol{DISH\rightarrow STOR}}(t) - \dot{\boldsymbol{Q}}_{\boldsymbol{STOR\rightarrow DEM}}(t)\right) \cdot \mathrm{dt} - \boldsymbol{\delta\kappa}^{\boldsymbol{ii}_2}_{\boldsymbol{STOR}} \quad \forall t \in \mathbf{T} \setminus \{1\} \tag{5}$$

The constant thermal loss term depends on the storage surface area and the external temperatures.

$$\begin{aligned}&\delta\boldsymbol{\kappa}^{\boldsymbol{ii}_2}_{\boldsymbol{STOR}} = \begin{cases} \boldsymbol{\kappa}^{\boldsymbol{ii}_2}_{\boldsymbol{STOR}} & \left| \; \boldsymbol{Q}^{\boldsymbol{ii}}_{\boldsymbol{STOR}} > 0 \right. \\ 0 & \left| \; \boldsymbol{Q}^{\boldsymbol{ii}}_{\boldsymbol{STOR}} = 0 \right. \end{cases} \\ &\boldsymbol{\kappa}^{\boldsymbol{ii}_2}_{\boldsymbol{STOR}} = \mathrm{U}_{\mathrm{STOR}} \cdot A^{out}_{STOR} \cdot \left(\mathrm{T}_{\mathrm{STOR}} - \mathbf{T}_{\mathbf{ext}}\right)\end{aligned} \tag{6}$$

Since the storage temperatures alternate between 65 and 85°C, the temperature T_{STOR} is conservatively chosen as constant 80°C. The hourly external temperature vector $\mathbf{T_{ext}}$ is given from the BSRN data. The storage outside surface area is a decision variable that depends on the storage volume. The volume is related to the storage maximum heat content by the heat capacity, the density and the total temperature change inside the tank.

Since the storage surface area is a non-linear function of the volume, it was linearly fit. Derivation of the coefficients is illustrated in Appendix A.

$$V_{STOR} = \frac{Q_{STOR}^{\max}}{c_p \cdot \rho \cdot \left(T_{STOR}^{h} - T_{STOR}^{c}\right)} \tag{7}$$

$$A_{STOR}^{out} = \alpha_{STOR} \cdot V_{STOR} + \beta_{STOR}$$

The constant thermal losses are only active if the storage is filled. The if-else-condition can only be represented in MILP by adding new binary variables $\boldsymbol{\delta_{STOR}} \in \{0,1\}$. Epsilon ε represents a very small number.

$$\begin{aligned} \boldsymbol{\delta_{STOR}} &\geq \boldsymbol{Q_{STOR}^{ii}} / Q_{STOR}^{MAX} \\ \boldsymbol{\delta_{STOR}} &\leq \boldsymbol{Q_{STOR}^{ii}} / \varepsilon \end{aligned} \tag{8}$$

With this the loss coefficient is derived by multiplication $\delta\boldsymbol{\kappa}_{\boldsymbol{STOR}}^{\boldsymbol{ii_2}} = \boldsymbol{\delta_{STOR}} \cdot \boldsymbol{\kappa}_{\boldsymbol{STOR}}^{\boldsymbol{ii_2}}$. Multiplication of a binary and a continuous variable can be formulated in MILP as a set of linear equations. Therefore, equation (6) is reformulated with $\kappa_{STOR}^{ii_2,MAX} = U_{STOR} \cdot A_{STOR}^{out,MAX} \cdot \left(T_{STOR} - T_{ext}^{min}\right)$ to the following.

$$\delta\boldsymbol{\kappa}_{\boldsymbol{STOR}}^{\boldsymbol{ii_2}} \geq \kappa_{STOR}^{ii_2,min} = 0 \tag{9}$$

$$\delta\boldsymbol{\kappa}_{\boldsymbol{STOR}}^{\boldsymbol{ii_2}} \leq \boldsymbol{\delta_{STOR}} \cdot \kappa_{STOR}^{ii_2,MAX} \tag{10}$$

$$\delta\boldsymbol{\kappa}_{\boldsymbol{STOR}}^{\boldsymbol{ii_2}} \leq \boldsymbol{\kappa}_{\boldsymbol{STOR}}^{\boldsymbol{ii_2}} = U_{STOR} \cdot A_{STOR}^{out} \cdot \left(T_{STOR} - \mathbf{T_{ext}}\right) \tag{11}$$

$$\boldsymbol{\kappa}_{\boldsymbol{STOR}}^{\boldsymbol{ii_2}} - \delta\boldsymbol{\kappa}_{\boldsymbol{STOR}}^{\boldsymbol{ii_2}} \leq \left(1 - \boldsymbol{\delta_{STOR}}\right) \cdot \kappa_{STOR}^{ii_2,MAX} \tag{12}$$

2.3.3.3 Storage model (iii)

Since the storage tank top temperature drops throughout the discharge cycle, the discharge demand cannot stay constant. To account for that constraint a third storage model is derived. The main difference from (ii) is one additional equation. After the charge cycle has finished, the storage discharge heat rate is constrained to be smaller or equal to a fraction of the previous discharge rate. The energy balance is based on model (ii) with equations (6)-(12).

$$\boldsymbol{Q_{STOR}^{iii}}(t) = \boldsymbol{Q_{STOR}^{iii}}(t-1) \cdot \kappa_{STOR}^{iii_1} + \left(\dot{\boldsymbol{Q}}_{\boldsymbol{DISH \rightarrow STOR}}(t) - \dot{\boldsymbol{Q}}_{\boldsymbol{STOR \rightarrow DEM}}(t)\right) \cdot \mathrm{dt} - \boldsymbol{\delta\kappa_{STOR}^{iii_2}} \quad \forall t \in \mathbf{T} \backslash \{1\} \tag{13}$$

The additional constraint on the discharge heat rate is valid two time steps after the charge period is finished.

$$\dot{\boldsymbol{Q}}_{\boldsymbol{STOR \rightarrow DEM}}(t) \leq \kappa_{STOR}^{iii_3} \cdot \dot{\boldsymbol{Q}}_{\boldsymbol{STOR \rightarrow DEM}}(t-1) + \dot{\boldsymbol{Q}}_{\boldsymbol{STOR \rightarrow DEM}}(t-2) \cdot 100 \qquad \forall t \in \mathbf{T} \backslash \{1,2\} \tag{14}$$

$$0 \leq \kappa_{STOR}^{iii_3} \leq 1 \tag{15}$$

2.3.3.4 Decision variables

In this work, the only fixed size is the area of the one solar collector. The storage volume (V_{STOR}), the industrial demand ($mult_{DEM}$) and all heat rates are decision variables. The solar fraction is defined as the ratio between the industrial demand and the peak solar thermal power output.

$$sf = \frac{mult_{DEM} \cdot \dot{Q}_{DEM}}{\dot{Q}_{DISH}^{\max}} \tag{16}$$

Another quantity that allows quantification of the solar part with respect to the total consumption is defined. The solar contribution (Ψ_{SOLAR}) represents the fraction of the solar dish output of the total yearly energy supply.

$$\psi_{DISH} = \sum_{t \in \mathbf{T}} \dot{\mathbf{Q}}_{\mathbf{DISH}} \Bigg/ \left(\sum_{t \in \mathbf{T}} \dot{\mathbf{Q}}_{\mathbf{DISH}} + \sum_{t \in \mathbf{T}} \dot{\boldsymbol{Q}}_{\boldsymbol{AUX}}(t) \right) \tag{17}$$

2.3.3.5 Objective function

The linear objective of the MILP is minimization of the global energetic losses. These are derived by summing the solar collector dish output and the total primary auxiliary consumption (an efficiency is attributed) and

subtracting the industrial demand consumption. This is a similar definition as the optimization of operational costs, but with purely energetic objectives. Since the solar input is constant, it has no influence on the optimization. The storage size is also taken into account in the objective function.

$$\min_{\substack{mult_{LOAD} \\ V_{STOR}}} f = \sum_{t\in\mathbf{T}} \dot{\mathbf{Q}}_{\mathbf{DISH}} + \sum_{t\in\mathbf{T}} \dot{\boldsymbol{Q}}_{\boldsymbol{AUX}}(t)/\eta_{\mathrm{AUX}} - \sum_{t\in\mathbf{T}} \dot{\mathrm{Q}}_{\mathrm{DEM}} \cdot mult_{DEM} + Q_{STOR}^{\max}/365 \tag{18}$$

2.4. Linear model parameter estimation methodology

The parameters of the storage models $\kappa^{i}_{\mathrm{STOR}}$, $\kappa^{ii1}_{\mathrm{STOR}}$, $\kappa^{iii1}_{\mathrm{STOR}}$, $\kappa^{iii3}_{\mathrm{STOR}}$ are determined with the Matlab® function *fmincon* that relies on sequential quadratic programming (SQP).
After it is ensured that the TRNSYS model follows the optimal control strategy in agreement with the MILP, the linear behavior is reconstructed in Matlab. All the variables (such as sizing of the components) are fixed and only the error parameters are left as decision variables for fmincon (see Fig. 2). To best imitate the TRNSYS behavior the objective function is set as the sum of the global error between the linear model and the TRNSYS data for the storage content and the auxiliary consumption. The quadratic hourly error is also investigated, but with less satisfying results. In this way the loss related parameters are determined for the location of Sede Boqer, see Table 2.

$$\min_{\substack{\kappa^{i}_{STOR} \\ \kappa^{ii1}_{STOR} \\ \kappa^{iii1}_{STOR},\kappa^{iii3}_{STOR}}} f = \sum_{t\in\mathbf{T}} \mathbf{Q}^{\mathbf{TRNSYS}}_{\mathbf{STOR}}(t) - \boldsymbol{Q}^{\boldsymbol{MILP}}_{\boldsymbol{STOR}}(t) + \sum_{t\in\mathbf{T}} \dot{\mathbf{Q}}^{\mathbf{TRNSYS}}_{\mathbf{AUX}}(t) - \dot{\boldsymbol{Q}}^{\boldsymbol{MILP}}_{\boldsymbol{AUX}}(t) \tag{19}$$

3. Results and discussion

3.1. Comparison between TRNSYS and MILP ($mult_{DEM}$ = 1)

In this chapter the results from the dynamic simulation in TRNSYS and the surrogate functions of the MILP are compared for a fixed demand ($mult_{DEM}$) size of one. That means that the solar fraction is set to 0.45, while the storage size, and the flow rates are left as decision variables. The TRNSYS output is generated based on the design and operation specifications from the MILP. The system performances are compared based on the auxiliary heater consumption and the hourly storage filling. Comparison of the computational effort is clearly decided by the MILPs which take between less than a minute (i), 10 min (ii), and 30 min (iii) compared to more than 5 hours per run for the TRNSYS model (however for different data resolution).

Fig. 3 (a) shows the heat demands and storage content of the TRNSYS simulation for Sede Boqer with a storage volume of 3.0m^3 compared to the MILP results with optimal volumes of 3.05m^3 (i), 3.15 m^3 (ii), and 3.05 m^3 (iii). The solar output, and amount sent to the storage and to the industrial demand are very similar between the TRNSYS and MILP formulation. For the TRNSYS data, the heat rate sent during discharge from the storage to the industrial demand shows a smooth constant reduction, while the MILP streams remain constant and then drop abruptly. This has an influence also on the hourly storage content, which in case of the MILP is emptied earlier than the TRNSYS. The storage content of the TRNSYS data is calculated by spacial integration over all storage node temperatures above 60°C.

The smoothest reduction of the MILP models can be observed for case (iii), however only slightly different from the other two. The temperatures in Fig. 3 (b) show the average temperature in the storage tank and the solar collector outlet temperature. The average storage temperature increases as expected throughout the day and drops during discharge. The solar outlet temperature is kept quite constant through the day and drops during the night.

As expected and implemented in TRNSYS, the MILP functions prioritize directly feeding the demand from solar energy before filling the storage. This is related to the thermal losses within the storage.

The error between TRNSYS and MILP total yearly auxiliary consumption is between -1 and -2.5% (see Table 3). Since the parameters are optimized for the case of Sede Boqer, it is important to test the correlations for a different location. The same test problem is run for weather data of Tateno, except from the storage volume which is adopted

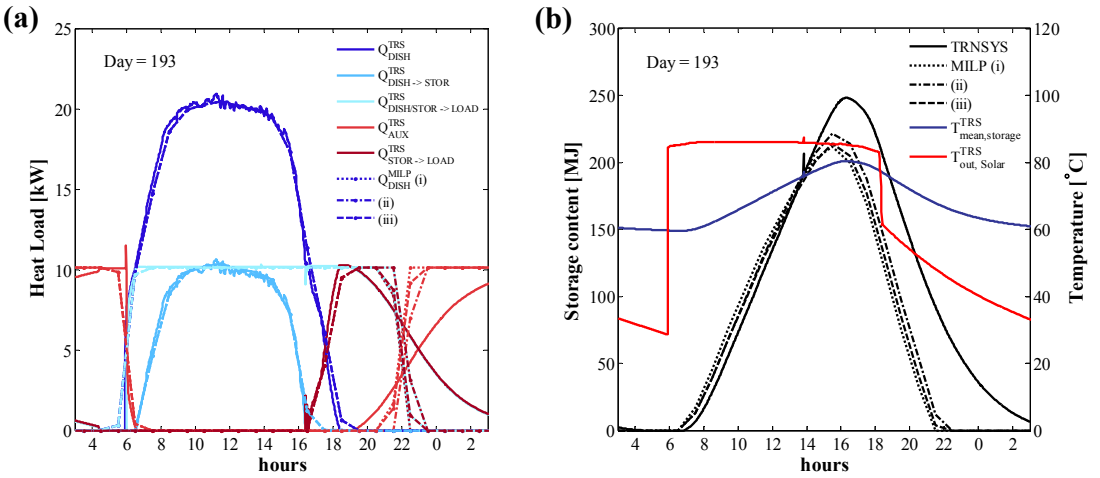

Fig. 3 Heat demands (a) and storage content (b) of TRNSYS simulation of Sede Boqer with storage tank volume of 3m^3 and MILP formulations with an optimal size of 3.05m^3 (i), 3.15 m^3 (ii), and 3.05 m^3 (iii) respectively for a fixed demand of $mult_{DEM}$=1.

from the MILPs (2.53m^3 (i), 2.55m^3 (ii), and 2.48m^3 (iii)) to be 2.5m^3. According to the values (depicted in Table 3) the deviation between TRNSYS and MILP for Tateno is between -4 and -5%, and therefore slightly higher than for Sede Boqer. It is suggested that this outcome stems from the thermal inertia of the storage tank and with that the dynamic behavior. In the MILP formulation this is not considered. It should have a bigger influence for regions with lower yearly DNI. However, the error of both locations for quite a high range of yearly DNI (2208 vs 1164 kWh/m^2) lies within the range of -1 and -5%. The smallest errors are achieved for the MILP model (iii) which however demonstrates the highest computational cost, followed by model (ii) with the second highest computational effort.

Fig. 4 illustrates a scatter plot of TRNSYS data and the MILP surrogate function of the hourly storage content for a fixed demand $mult_{DEM}$ of 1, for Sede Boqer and Tateno. The slopes of the linear fits of Sede Boqer are slightly below 1 while the ones from Tateno are slightly above 1. This is explained again by the fact that the MILP does not consider the dynamic losses and therefore overestimates the storage content of locations with lower, or more variable DNI. For high and constant DNI regions, as Sede Boqer, the surrogate function tends to underestimate the storage content slightly. But all in all, the agreement is considered sufficient for a demand multiplication factor of 1.

Finally, the monthly mean heat rates of the TRNSYS model and MILP are compared in Fig. 5 for a storage tank volume of 3m^3 and 3.05 m^3 (iii). It shows that the MILP overestimates the solar and storage output in winter and underestimates in summer for Sede Boqer, and it most of the time overestimates the values for Tateno. That explains, why the MILP data for Sede Boqer agrees quite well (-0.9%) with the TRNSYS and for Tateno it deviates a more (-4.1%). It also illustrates that even if the solar fraction is the same, solar contribution (Ψ_{SOLAR}) of Sede Boqer is much higher than that of Tateno with 0.5 and 0.27 respectively. This is clearly related to the approximately two times higher yearly DNI in Sede Boqer compared to Tateno. It further indicates that adequate sizing of the solar system is an interesting issue that may depend on the geographic region.

Summarizing this subchapter, it can be said:

- The MILPs take between less than a minute (i), 10 min (ii), and 30 min (iii) compared to more than 5 hours per run for the TRNSYS
- The general agreement between MILP and TRNSYS output is sufficient for the estimation of the yearly (and monthly) auxiliary heat consumption and the storage content.
- The MILP consequently underestimates the auxiliary consumption (between -0.9% and -5.0%). It is more precise for Sede Boqer than Tateno.
- The three MILP models yield quite similar results. The descending order of precision is (iii)→(ii)→(i), which represents the inverted order of the computational time.
- For low DNI regions the MILP models tend to overestimate the storage content, while for high DNI regions they tend to underestimate.

Table 3 TRNSYS and MILP yearly total auxiliary heat demand for the locations Sede Boqer and Tateno in 2011.

MWh	TRNSYS	(i)	(ii)	(iii)	% (i)	% (ii)	% (iii)
Sede Boqer	48.0	46.9	47.0	47.63	-2.4	-2.2	-0.9
Tateno	68.7	65.3	65.7	65.9	-5.0	-4.4	-4.1

3.2. Demand sizing

The optimal size of the demand for one collector dish is investigated with regard to the objective function which aims at minimizing the total energetic losses.

Fig. 6 displays the objective function of the TRNSYS and MILP outputs for different storage and solar fractions of the locations of Sede Boqer and Tateno. One important note is that the chosen storage size has a non-negligible influence on the TRNSYS output (auxiliary heat consumption). As an example, for a solar fraction of 0.23 in Tateno, from the empirical rule (parenthesis) a storage of 5.5m^3 is proposed and from the MILPs a storage size of 4m^3 is suggested. In TRNSYS the sizes 9 and 4m^3 were run showing that the objective function can be reduced by 20%. This can be explained with the relation between the thermal losses and the storage outside surface area.

For Sede Boqer the optimal solar fration given by the MILP ranges from 0.39 (i) to 0.43 (ii). This indicates that the original choice of sizing (sf=0.45) is close to the MILP optimum. For the case of Tateno, however, a solar fraction between 0.18 (i) and 0.23 (ii) is recommended for the given problem. Model (i) shows the strongest deviation from the TRNSYS data. That can be seen for Sede Boqer (errors at sf=0.36 (i) -7.2%, (ii) -6.8%, (iii) -0.9%, at 0.6 (for different volumes) (i) -15.6%, (ii) -14.1%, (iii) -12.6%), and for Tateno (errors at sf=0.23 (i) -16.0%, (ii) -9.3%, (iii) -4.5%). Therefore, model (ii) is proposed as best suited for targeting optimal design. It is derived that model (iii) is more accurate than (ii) at higher computational cost and cannot be evaluated below certain sizes (0.45).

However, with increasing distance from the MILP optimum, the MILP results converge to the same values and diverge more strongly from the TRNSYS results. It is still inferred that the MILPs, especially model (ii), follow the same trend as the TRNSYS model and it will give a good first estimate of the objective function minimum and auxiliary consumption. In the demonstrated example the sizing and system complexity is quite trivial, but in a more elaborated scenario, such as shown in references (21, 24), these functions could be applied for good estimates of the here discussed components. In order to increase the significance and the applicability of the presented results, a wider range of temperature levels and collectors may be studied. This will however not replace a thorough dynamic analysis, but it may postpone it.

Fig. 7 illustrates different MILP optimal solar fractions for BSRN stations of various yearly DNI values. A clear trend is recognizable for increasing DNI the optimal solar fraction increases. A solar contribution of around 0.5 seems the most favorable for all locations.

From the results above, it is condensed:

- Model (ii) is proposed as best suited for targeting optimal design and control.
- The derived functions can be applied for good estimates in more complex MILP optimization.
- The MILP models follow the same trend as the TRNSYS data and give a good estimate of the objective function minimum and auxiliary consumption.
- With increasing distance from the MILP optimum, the MILP results converge to the same values and diverge more strongly from the TRNSYS results.
- The MILP models cannot replace a thorough dynamic analysis, but they may postpone it.
- As expected with increasing DNI the optimal solar fraction increases such that the solar contribution converges to 0.5.

4. Conclusions and outlook

The challenge between sufficient accuracy at reasonable computational time is tackled in this work for three different MILP models (i)-(iii) for a solar thermal system coupled with a stratified thermal storage tank to supply heat to a continuous industrial process. The process is represented by a constant demand. A TRNSYS model of the

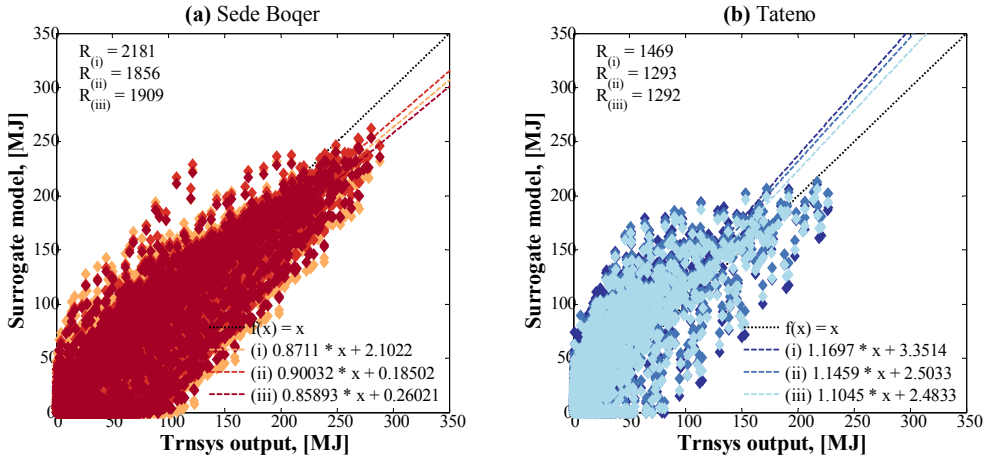

Fig. 4 Scatter plot of hourly storage content of TRNSYS model with storage tank volume of 3m^3 and MILP surrogate function with an optimal size of 3.05/ 2.54m^3 (i), 3.15/ 2.56m^3 (ii), and 3.05/ 2.48m^3 (iii) respectively for Sede Boqer/Tateno, at a fixed demand of $mult_{DEM}$=1.

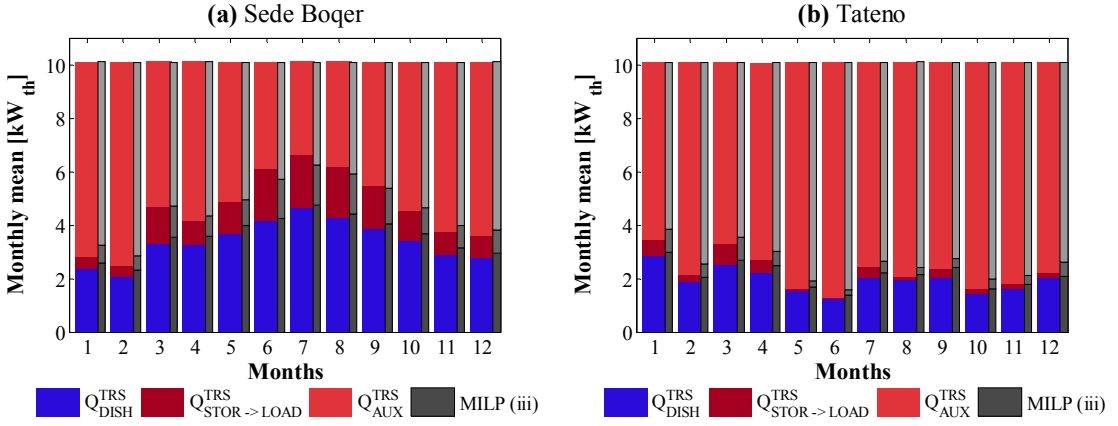

Fig. 5 Monthly mean data of the thermal power directly transferred from the solar dish to the demand, the storage output towards the demand, and the auxiliary demand of the TRNSYS data a storage tank volume of (a) 3m^3, (b) 2.5m^3 and MILP (a) 3.05 m^3 (iii), (b) 2.48m^3 for a fixed demand of $mult_{DEM}$=1.

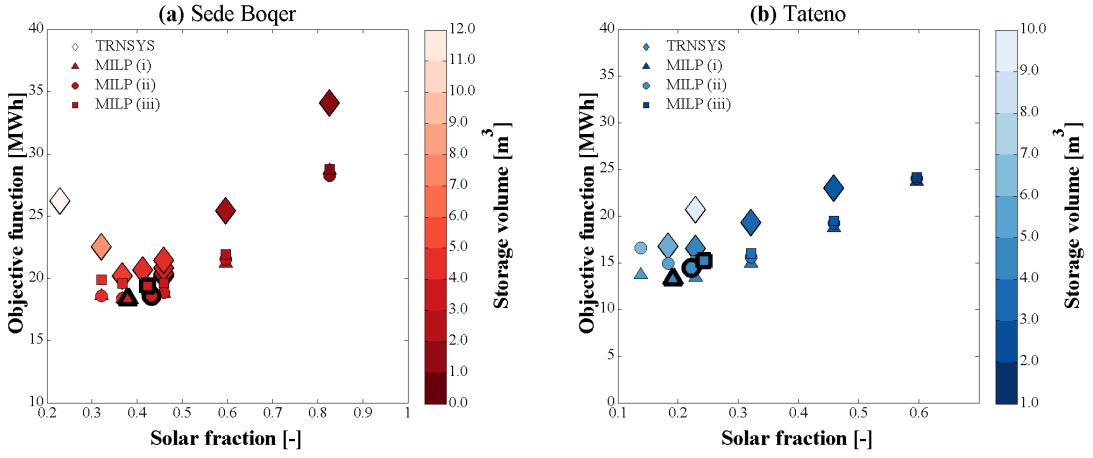

Fig. 6 Objective function for TRNSYS and MILP outputs for different storage and demand sizes. The thick lines mark the MILP minimum for two decision variables (V_{STOR}, $mult_{DEM}$), while the thin lines mark points with a fixed demand size ($mult_{DEM}$ fixed).

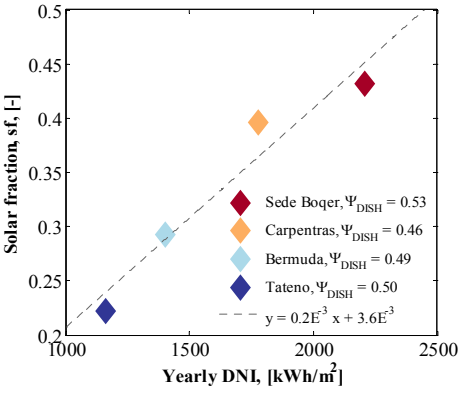

Fig. 7 MILP optimal solar fraction for different BSRN stations of various yearly DNI values.

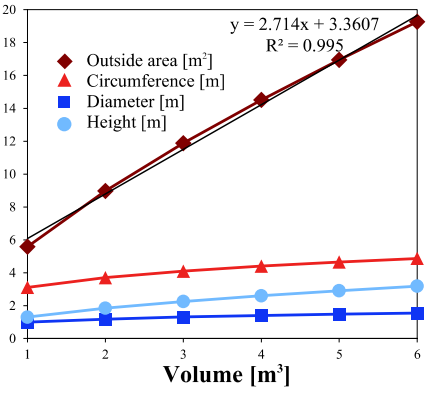

Fig. 8 Outside area, circumference, diameter, and height versus tank volume.

same problem is created and used for tuning of parameters in the MILP formulation (for the location of Sede Boqer) as well as for testing the optimal set of decision variables (Sede Boqer, Tateno).

The MILPs take between less than a minute (i), 10 min (ii), and 30 min (iii) compared to more than 5 hours per run for the TRNSYS model. It is concluded that the general agreement between MILP and TRNSYS output is sufficient for an estimation of the yearly (and monthly) auxiliary heat consumption (-1 to -5%). The MILP storage content tends to be slightly overestimated for the low DNI region (Tateno), while for the high DNI region (Sede Boqer) it is underestimated. The descending order of precision of the MILPs starts with model (iii) through (ii) towards (i), which represents the inverted order of the computational time. For differently chosen decision variable values, the MILP models follow the same trend as the TRNSYS data and give a good estimate of the objective function minimum and auxiliary consumption. Model (ii) is proposed as best suited for targeting optimal design and control.

For future investigations it is recommended to study more complex TRNSYS models (e.g. including cooling coils, or a more complex solar field design) and more locations. In order to increase the significance and the applicability of the presented results, a wider range of storage and collector temperature levels and types may be studied.

Further, a reduction of the radiation data to a set of typical (sequential) periods (34, 35) could be an option which allows for more complex MILP (storage) models (25). In this first analysis this option is excluded in order to keep origin of the system errors traceable. Finally, the goal of this work is not the replacement of thorough dynamic analysis by MILP, but maybe a postponement.

Acknowledgements

The contribution from Airlight Energy SA (31) is gladly acknowledged in this work.

Appendix A. Linear fit of storage tank outside area

The cylindrical storage tank outside surface area is linearly fit to the storage volume. The storage height is derived from a fixed predefined ratio between the cross-sectional area and the height $h = \sqrt{V} \cdot 1.3$.
Another way of deriving the storage height is by fixing the height to diameter ratio. Ratios between 1 and 3 are recommended for stratified tanks (36), but are not discussed here, since the influence turned out to be marginal.

The outside surface area is calculated as a function of the tank volume and height.

$$A^{out} = h \cdot \pi \cdot \underbrace{\sqrt{V/h \cdot 4/\pi}}_{d} + 2 \cdot V/h \qquad (20)$$

For a volumetric range between 1 and 6 m^3 the above non-linear function is plotted and fitted linearly (see Fig. 8).

The linear coefficients of the storage tank outside area, the slope and intercept, are fit as $\alpha_{STOR} = 2.714$ and $\beta_{STOR} = 3.3607$, respectively.

References

[1] Henning H-M. Solar assisted air conditioning of buildings – an overview. Applied Thermal Engineering. 2007;27:1734-49.
[2] Klein SA, Beckman WA, Mitchell JW, Duffie JA, Duffie NA, Freeman TL. TRNSYS 16. 2006.
[3] Kalogirou SA, Tripanagnostopoulos Y. Industrial application of PV/T solar energy systems. Applied Thermal Engineering. 2007 6//;27(8–9):1259-70.
[4] Kalogirou SA, Tripanagnostopoulos Y. Hybrid PV/T solar systems for domestic hot water and electricity production. Energy Conversion and Management. 2006 11//;47(18–19):3368-82.
[5] Kalogirou SA. Optimization of solar systems using artificial neural-networks and genetic algorithms. Applied Energy. 2004 4//;77(4):383-405.
[6] Assilzadeh F, Kalogirou S, Ali Y, Sopian K. Simulation and optimization of a LiBr solar absorption cooling system with evacuated tube collectors. Renewable Energy. 2005;30(8):1143-59.
[7] Calise F, d'Accadia MD, Palombo A. Transient analysis and energy optimization of solar heating and cooling systems in various configurations. Solar Energy. 2010;84:432-49.
[8] Schumacher J. Digitale Simulation regenerativer elektrischer Energieversorgungssysteme [Dissertation]: Universität Oldenburg; 1991.
[9] Crawley DB, Lawrie LK, Winkelmann FC, Buhl WF, Huang YJ, Pedersen CO, et al. EnergyPlus: creating a new-generation building energy simulation program. Energy and buildings. 2001;33(4):319-31.
[10] Polysun 5.0. Rapperswil: Vela Solaris; 2009.
[11] Nguyen A-T, Reiter S, Rigo P. A review on simulation-based optimization methods applied to building performance analysis. Applied Energy. 2014;113:1043–58.
[12] B.M. Adams ea. DAKOTA, A Multilevel Parallel Object-Oriented Framework for Design Optimization, Parameter Estimation, Uncertainty Quantification, and Sensitivity Analysis: Version 5.0 User's Manual. Livermore, CA: Sandia National Laboratory, 2009.
[13] Wetter M, editor GenOpt-A generic optimization program. Seventh International IBPSA Conference, Rio de Janeiro; 2001.
[14] Zagrouba M, Sellami A, Bouaïcha M, Ksouri M. Identification of PV solar cells and modules parameters using the genetic algorithms: Application to maximum power extraction. Solar Energy. 2010 5//;84(5):860-6.
[15] Varun, Siddhartha. Thermal performance optimization of a flat plate solar air heater using genetic algorithm. Applied Energy. 2010 5//;87(5):1793-9.
[16] Boonbumroong U, Pratinthong N, Thepa S, Jivacate C, Pridasawas W. Particle swarm optimization for AC-coupling stand alone hybrid power systems. Solar Energy. 2011 3//;85(3):560-9.
[17] Mellit A, Kalogirou SA, Hontoria L, Shaari S. Artificial intelligence techniques for sizing photovoltaic systems: A review. Renewable and Sustainable Energy Reviews. 2009 2//;13(2):406-19.
[18] Becker HC. Methodology and Thermo-Economic Optimization for Integration of Industrial Heat Pumps: EPFL; 2012.
[19] Wallerand AS, Albarelli JQ, Ensinas AV, Ambrosetti G, Mian A, Marechal F. Multi-objective Optimization of a Solar Assisted 1st and 2nd Generation Sugarcane Ethanol Production Plant. Proceedings of ECOS 2014. 2014.
[20] Mian A, Bendig M, Piazzesi G, Manente G, Lazzaretto A, Marechal F. Energy Integration in the cement industry. In: Kraslawski A, Turunen I, editors. 23rd European Symposium on Computer Aided Process Engineering (ESCAPE); June 9-13, 2013; Lappeeranta, Finland. Amsterdam: Elsevier Science Bv; 2013. p. 349-54.
[21] Ashouri A, Fux SS, Benz MJ, Guzzella L. Optimal design and operation of building services using mixed-integer linear programming techniques. Energy. 2013 9/15/;59(0):365-76.
[22] Fux SF, Benz MJ, Guzzella L. Economic and environmental aspects of the component sizing for a stand-alone building energy system: A case study. Renewable Energy. 2013 7//;55(0):438-47.
[23] Fazlollahi S, Mandel P, Becker G, Maréchal F. Methods for multi-objective investment and operating optimization of complex energy systems. Energy. 2012 9//;45(1):12-22.
[24] Girardin L. A GIS-based Methodology for the Evaluation of Integrated Energy Systems in Urban Area: EPFL; 2012.
[25] Fazlollahi S, Becker G, Maréchal F. Multi-objectives, multi-period optimization of district energy systems: II—Daily thermal storage. Computers & Chemical Engineering. 2013.
[26] Schütz T, Streblow R, Mülle D. A comparison of thermal energy storage models for building energysystem optimization. Energy and Buildings. 2015;93:23-31.
[27] Campos Celador A, Odriozola M, Sala JM. Implications of the modelling of stratified hot water storage tanks in the simulation of CHP plants. Energy Conversion and Management. 2011 8//;52(8–9):3018-26.
[28] Bemporad A, Morari M. Control of systems integrating logic, dynamics, and constraints. Automatica. 1999 3//;35(3):407-27.
[29] Selviaridis A, Burg BR, Wallerand AS, Maréchal F, Michel B. THERMO-ECONOMIC ANALYSIS OF A TRIGENERATION HCPVT POWER PLANT. CPV conference Proceedings. 2015.
[30] Selviaridis A. System Modeling and Thermo-Economic Analysis of a High Concentration Photovoltaic Thermal System. Lausanne: Ecole Polytechnique Federale de Lausanne; 2014.
[31] Airlight Energy SA [02.10.2014]. Available from: http://www.airlightenergy.ch/.
[32] Ohmura A, Gilgen H, Hegner H, Müller G, Wild M, Dutton EG, et al. Baseline Surface Radiation Network (BSRN/WCRP): New precision radiometry for climate research. Bulletin of the American Meteorological Society. 1998;79(10):2115-36.

[33] Klein S, Beckman W, Mitchell J, Duffie J, Duffie N. TRNSYS 17 reference manual. Madison: Solar Energy Laboratory, Univ of Wisconsin-Madison. 2005.
[34] Fazlollahi S, Bungener SL, Mandel P, Becker G, Maréchal F. Multi-objectives, multi-period optimization of district energy systems: I. Selection of typical operating periods. Computers & Chemical Engineering. 2014 6/4/;65(0):54-66.
[35] Bungener S, Hackl R, Van Eetvelde G, Harvey S, Marechal F. Multi-period analysis of heat integration measures in industrial clusters. Energy. 2015 12/15/;93, Part 1:220-34.
[36] Ochs F. Modelling large-scale thermal energy stores: Faculty of Energy and Process and Bio Technology, University of Stuttgart; 2009.